Turkish Journal of Chemistry

http://journals.tubitak.gov.tr/chem/

Research Article

Turk J Chem
(2019) 43: 63 – 72
© TÜBİTAK
doi:10.3906/kim-1807-6

# Synthesis of highly active crystalline carbon nitride prepared in various salt melts for photocatalytic degradation of phenol

**Mohd Hayrie MOHD HATTA**[1], **Hendrik Oktendy LINTANG**[2,3,4], **Siew Ling LEE**[1,4], **Leny YULIATI**[2,3,4,*]

[1]Department of Chemistry, Faculty of Science, Universiti Teknologi Malaysia, UTM Johor Bahru, Johor, Malaysia
[2]Ma Chung Research Center for Photosynthetic Pigments, Universitas Ma Chung, Malang, East Java, Indonesia
[3]Department of Chemistry, Faculty of Science and Technology, Universitas Ma Chung, Malang, East Java, Indonesia
[4]Center for Sustainable Nanomaterials, Ibnu Sina Institute for Scientific and Industrial Research, Universiti Teknologi Malaysia, UTM Johor Bahru, Johor, Malaysia

**Received:** 03.07.2018 • **Accepted/Published Online:** 02.10.2018 • **Final Version:** 05.02.2019

**Abstract:** Crystallinity could have a decisive influence on photocatalytic performance. In this study, the synthesis of crystalline carbon nitride (CN) was studied via an ionic melt polycondensation of urea precursor in the presence of various salt melts, which were KCl-LiCl, KCl-NaCl, and KCl-$ZnCl_2$. While all the salt melts helped to improve the optical properties of the CN, only KCl-LiCl salt melt could form crystalline CN as evidenced by its X-ray diffraction pattern. Furthermore, the specific surface area of CN (72 $m^2$/g) was maintained when using KCl-LiCl (73 $m^2$/g), but it was decreased in the presence of KCl-NaCl (22 $m^2$/g) or KCl-$ZnCl_2$ (17 $m^2$/g). The CN prepared without the salt melt only showed 10% phenol degradation under the light of a solar simulator, while the use of KCl-LiCl significantly improved the activity to 24%. On the other hand, the CN prepared in the presence of KCl-NaCl and KCl-$ZnCl_2$ gave phenol degradation of 14% and 7%, respectively. This work demonstrated that the crystallinity, improved absorption in the visible light region, and maintained large specific surface area of the CN were crucial to achieve the high activity.

**Key words:** Carbon nitride, crystallinity, KCl-LiCl, phenol, salt melt

## 1. Introduction

Graphitic carbon nitride (CN) is a class of polymeric materials consisting of carbon (C) and nitrogen (N) elements[1] that have been found to have many applications in catalysis field, such as acting as electrocatalysts, oxidation catalysts, and catalyst supports, as well as in material fields such as nanocomposite fillers.[2] Recently, CN has attracted significant attention to the photocatalysis field owing to its stability and good activities for various photocatalytic reactions under ultraviolet (UV) and visible light irradiation.[3–7] In particular, the capability of CN to work under visible light is crucial as our sunlight consists of more visible light than UV light. However, most of the synthesized graphitic CN was found to have less ordered structure and be in an amorphous phase.[3–8] For most applications in the photocatalysis field, the organized structure of molecules or the crystallinity would affect the electron flow.[9] In other words, the photocatalytic performance is notably affected by the crystallinity of the photocatalyst used in the reaction.[10] However, even though it is a promising approach, constructing a crystalline photocatalyst that is able to reduce the electron-hole recombination and

*Correspondence: leny.yuliati@machung.ac.id

works excellently under the visible light region is a challenging and difficult task. Typically, a crystalline CN material that has a well-defined morphology and large surface area can be synthesized using LiX/KX salt melts (X = Cl, Br) as the reaction media.[10−12]

The use of salt melt as a medium for chemical processes can be tracked back to the 1960s, when molten salts were found as effective reaction media to synthesize some organic compounds.[13,14] Among the chemicals that were successfully synthesized were silicon and carbon cyanates, thiocyanates, and cyanides, as well as some pseudohalogenides consisting of carbonyl and fluorocarbonyl groups.[15] This successful chemical preparation proved that salt melts have good solvating properties. This approach could be suitable for the synthesis of CN, because salt melts usually have good stability at high temperature and the polycondensation point of s-heptazine is relatively higher than the melting point of the salt melts. Furthermore, in order to facilitate the polymerization of the precursor to form the CN network, the precursor shall be solvated by the salt melt.[16] In this study, the use of potassium chloride (KCl)-based salt melts was examined to produce crystalline CN since KCl could decrease the temperature of the melting point of the salt melt.

On the other hand, phenol has been recognized as one of the most common organic pollutants in wastewater. As wastewater and groundwater containing phenol may cause contamination and have a negative effect on the ecosystem and humans, therefore, the complete removal of phenol from wastewater is required before its disposal into the environment.[17] Due to its toxicity even at low concentrations and the ability of phenol to easily form some substituted intermediates during the oxidation process, many researchers have focused on developing efficient techniques for phenol removal. Since phenolic compounds are nonbiodegradable and the adsorption method is less favorable due to its high cost,[18] advance oxidation processes (AOPs) have become some of the best options for wastewater treatment. AOPs work well to eliminate and remove various toxic organic pollutants that are present in water and wastewater by reactions with hydroxyl radicals ($\bullet$ OH) via an oxidation process. In AOPs, the $\bullet$ OH would attack the organic pollutants forming an intermediate compound that eventually is converted into harmless compounds, which are mainly carbon dioxide ($CO_2$) and water ($H_2O$) as well as inorganic salts.[19] In the application of wastewater treatment, AOPs can be specifically termed as chemical processes that use ozone ($O_3$), ozone in combination with UV ($O_3$/UV), ozone with hydrogen peroxide ($O_3/H_2O_2$), hydrogen peroxide and UV ($UV/H_2O_2$), Fenton's reagent, and photocatalytic oxidation.[18−20] Among them, the photocatalytic oxidation method has been proposed as one of the most efficient and environmentally safe processes to degrade phenol pollutants.[21]

In this work, we explore the use of various salt melts for the preparation of crystalline CN, with the main objective of increasing the crystallinity of the CN so that the photocatalytic performance towards degradation of phenol is enhanced. To the best of our knowledge, there is still no report on the photocatalytic degradation of organic pollutants using crystalline CN. Following the successful improvement in photocatalytic hydrogen production using crystalline CN,[10] this work provides evidence of the significant improvement in the photocatalytic degradation of phenol using crystalline CN as compared to amorphous CN.

## 2. Results and discussion

### 2.1. Structural analysis

Figure 1 shows the X-ray diffraction (XRD) patterns of all the prepared CN samples. As can be seen in Figure 1a, the CN prepared from urea precursor was in amorphous form as it only showed broad peaks at $2\theta$ of 11.2° and 27.7°. The peak at ca. 27.7° could be indexed as the (002) plane, corresponding to the interplanar stacking

of conjugated aromatic rings. Meanwhile, another pronounced peak observed at ca. 11.2° would be related to the in-plane structural packing.[3−5,22,23]

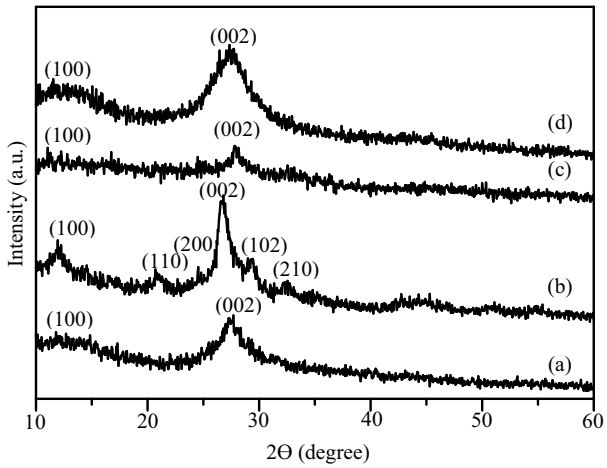


**Figure 1**. XRD patterns of (a) CN, (b) CN-KCl-LiCl, (c) CN-KCl-NaCl, and (d) CN-KCl-$ZnCl_2$.

When the CN was prepared in the presence of KCl-LiCl, additional peaks could be observed, as displayed in Figure 1b. The CN-KCl-LiCl gave diffraction peaks at $2\theta$ of 11.9°, 20.7°, 24.5°, 26.8°, 29.3°, and 32.4° due to the (100), (110), (200), (002), (102), and (210) planes, respectively.[16] This result confirmed the crystalline phase of the CN-KCl-LiCl, where the structure was similar to the reported poly(triazine imide)-like structure.[24] In contrast, the presence of KCl-NaCl was unable to increase the crystallinity of CN as shown in Figure 1c. The KCl-NaCl might not act as a reactive solvent since the condensation of the precursor to form the CN could start at a lower temperature as compared to the melting point of the KCl-NaCl.[25] As shown in Figure 1d, the addition of KCl-$ZnCl_2$ salt melt led to the formation of the amorphous phase. This was in good agreement with a previous study where the polycondensation process was carried out using melamine in the presence of KCl-$ZnCl_2$.[26]

### 2.2. Optical properties

Optical absorption properties of the prepared CN materials were investigated by diffuse reflectance (DR) UV-vis spectroscopy. As can be seen in Figure 2, three absorption peaks appeared mainly at 277, 340, and ~375 nm. The first absorption peak at 277 nm would indicate a $\pi \rightarrow \pi^*$ charge transfer at the C=N groups, while the n $\rightarrow \pi^*$ electronic transition owing to the formation of the C-N terminal groups could be observed at ~375 nm.[22,23] The absorption peak observed at 340 nm could be associated with the formation of C=O with $\pi \rightarrow \pi^*$ electronic transition.[22]

The main difference in the absorption properties of all the prepared CN samples was the shifting of some peaks. As shown in Figure 2a, the CN showed a visible light absorption up to ca. 430 nm. On the other hand, as depicted in Figures 2b, 2c, and 2d, other CN samples prepared in the presence of the salt melt gave significant shifting up to 460 nm. It has been reported that the redshift would be contributed by the larger delocalization of electrons in the sheets of CN, which could indicate the higher degree of condensation during the synthesis process.[3] This result showed that the presence of salt melt might improve the degree of precursor condensation. In addition to the large redshift, new peaks were observed at ca. 360 and 420 nm for

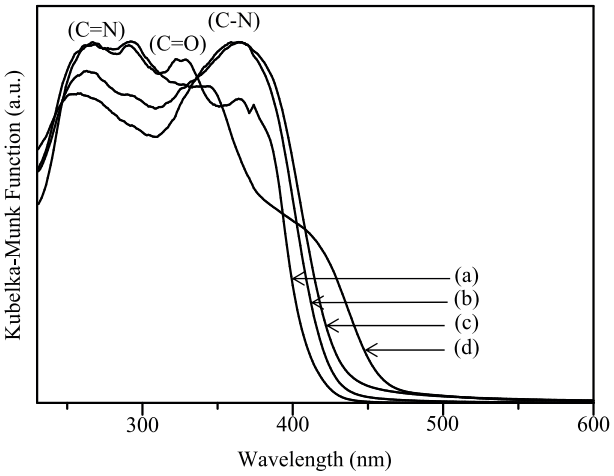


**Figure 2**. DR UV-vis spectra of (a) CN, (b) CN-KCl-LiCl, (c) CN-KCl-NaCl, and (d) CN-KCl-$ZnCl_2$.

the CN-KCl-$ZnCl_2$, owing to the presence of Zn species that might give a new charge transfer pathway,[21] but different from the one observed on ZnO-CN composites.[27,28] However, the improved optical properties of the CN samples prepared in the presence of the salt melt would not be the only important parameter affecting the photocatalytic performance.

### 2.3. Functional groups

The functional groups of all the CN samples were examined by Fourier transform infrared (FTIR) spectroscopy as displayed in Figure 3. The FTIR spectrum of the reference CN is shown in Figure 3a. The successful formation of CN network structure can be shown from the vibration bands around 810 and 1200–1600 $cm^{-1}$,[3,16,22,23,25] which corresponded to the characteristic bending mode of triazine units and typical stretching modes of CN heterocycles, respectively. In more detail, the bands observed at 1250, 1330, 1420, and 1460 $cm^{-1}$ were attributed to the stretching mode of CN heterocycles, while the band at 1636 $cm^{-1}$ was attributed to stretching mode of C=N. The broad bands observed in the region of 2400–3400 $cm^{-1}$ indicated the presence of surface hydroxyl groups (OH) and amino groups either in terminal or residual parts ($NH_2$ and NH).

As shown in Figures 3b, 3c, and 3d, the addition of salt melts during synthesis reaction caused broadening and subsequent overlap of the absorption band, while unmodified CN gave more defined vibration peaks in the range of 1200–1600 $cm^{-1}$. It can be noted that the addition of salt melts resulted in the appearance of a small peak at 2179 $cm^{-1}$, which was attributed to the formation of N=C=N or C≡N. This peak could be an indication that defects were formed in the CN networks when the CN was prepared in the presence of the salt melt. A less condensed framework has been also reported when using dicyandiamide as the precursor in the presence of a salt melt to prepare CN.[16]

### 2.4. Textural properties

Figure 4 shows the nitrogen $N_2$ adsorption-desorption isotherms for all the CN samples. As displayed in Figure 4a, the reference CN exhibited the isotherm type III for nonporous materials, but with the presence of a clear hysteresis loop at high relative pressure. This hysteresis loop suggested the presence of cavities such as mesopores generated from the interparticulate spaces. On the other hand, as shown in Figure 4b, the CN-KCl-

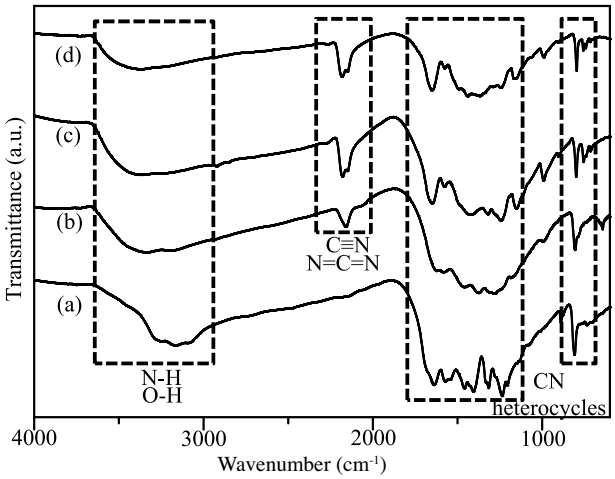


**Figure 3**. FTIR spectra of (a) CN, (b) CN-KCl-LiCl, (c) CN-KCl-NaCl, and (d) CN-KCl-$ZnCl_2$.

LiCl exhibited isotherm type IV according to the IUPAC classification. The isotherm of CN-KCl-LiCl consisted of a hysteresis loop with type H3 at the relative pressure ($P/P_0$) of 0.4, indicating the presence of a porous structure. The porous structure in the CN-KCl-LiCl could be formed due to the generation of channels having a zeolite-like porous structure as the result of the stacking between voids in the CN layers containing ions ($Li^+$ and $Cl^-$), as has been reported when using dicyandiamide as the precursor.[11] The Barret–Joyner–Halenda (BJH) pore diameter of the CN-KCl-LiCl was determined to be 3.62 nm, which indicated the mesoporosity in the CN-KCl-LiCl. It is worth noting that only the CN-KCl-LiCl has the clear character of mesopore structure, while the CN-KCl-NaCl and the CN-KCl-$ZnCl_2$, shown in Figures 4c and 4d, respectively, exhibited isotherm type III. Similar to the reference CN, these two materials also have clear hysteresis loops, suggesting the presence of mesopores generated from the interparticulate spaces.

The Brunauer–Emmett–Teller (BET) specific surface area values for all CN samples are summarized in Table 1. The specific surface area of the CN was 72 $m^2/g$ and it could be maintained high (73 $m^2/g$) for the case of the CN-KCl-LiCl sample. In contrast, the surface area of the CN dropped drastically to 22 and 17 $m^2/g$ when it was prepared in the presence of KCl-NaCl and the KCl-$ZnCl_2$ salt melts, respectively. The difference might be associated with the formation of porosity in the CN-KCl-LiCl sample mentioned above. In good agreement with the isotherm curves shown in Figures 4c and 4d, even though there were mesopores due to the cavities or interparticulate spaces, the absence of mesoporous structures on the CN-KCl-NaCl and CN-KCl-$ZnCl_2$ reflected the measured low values of the external surface area. The total pore volumes of all CN samples are also listed in Table 1. The addition of salt melts reduced the total pore volumes of the reference CN since the salt melts might block the large interparticulate spaces in the reference CN. However, the CN-KCl-LiCl clearly showed higher total pore volume than the CN-KCl-NaCl and the CN-KCl-$ZnCl_2$ owing to the formation of mesoporosity in the CN-KCl-LiCl.

### 2.5. Photocatalytic activity

The evaluation of the photocatalytic performance was conducted for photocatalytic degradation of phenol. The reaction was carried out for 6 h using the solar simulator as the light source. As shown in Table 2, the reference CN showed only 10% phenol degradation. The addition of the salt melts increased the activity of the CN,

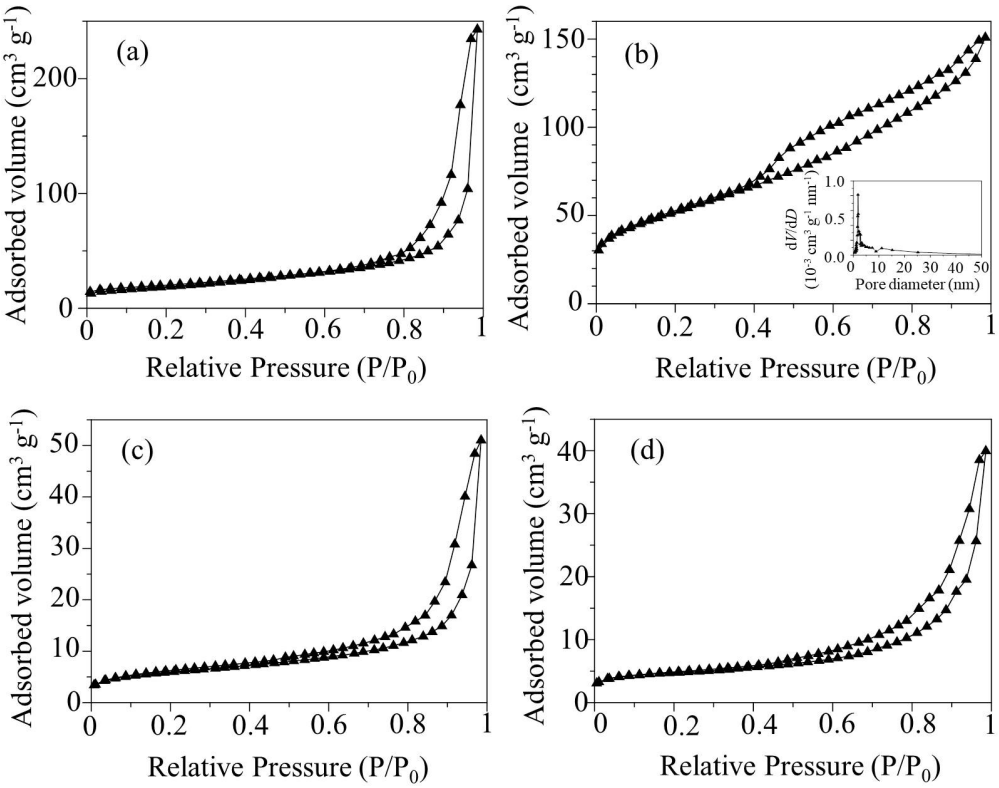


**Figure 4**. $N_2$ adsorption-desorption isotherms of (a) CN, (b) CN-KCl-LiCl, (c) CN-KCl-NaCl, and (d) CN-KCl-$ZnCl_2$. Inset shows the BJH pore size distribution of the CN-KCl-LiCl.

**Table 1**. BET specific surface area, pore diameter, and total pore volume of the prepared CN samples.

| Samples | Surface area ($m^2$/g) | Pore diameter (nm) | Total pore volume ($cm^3$/g) |
|---|---|---|---|
| CN | 72 | n.a. | 0.38 |
| CN-KCl-LiCl | 73 | 3.62 | 0.23 |
| CN-KCl-NaCl | 22 | n.a. | 0.08 |
| CN-KCl-$ZnCl_2$ | 17 | n.a. | 0.06 |

n.a.: Not applicable.

except for the CN-KCl-$ZnCl_2$. The highest activity was obtained on the CN-KCl-LiCl that demonstrated 24% phenol degradation, which was 2.4 times higher than the reference CN. On the other hand, the CN-KCl-$ZnCl_2$ showed lower photocatalytic activity than the CN (7%).

**Table 2**. Photocatalytic activity of the prepared samples.

| Samples | Activity (%) |
|---|---|
| CN | 10 |
| CN-KCl-LiCl | 24 |
| CN-KCl-NaCl | 14 |
| CN-KCl-$ZnCl_2$ | 7 |

The improved photocatalytic degradation on the CN-KCl-LiCl sample was mainly due to its high crystallinity, improved optical property in the visible region, and large surface area as compared to the CN samples prepared in the presence of other salt melts. The higher crystallinity would lead to better mobility of charge carriers. As has been reported elsewhere,[10] the efficient flow of electron transfer in the crystalline and well-ordered arrangement of the CN gave a good influence on the photocatalytic performance of the CN. In addition, the maintained large surface area of the CN-KCl-LiCl would also give a positive impact on its performance.

**Table 3**. The composition of salt melts in the synthesis method.

| Salt melt | Weight of KCl (g) | Weight of M-Cl (g) |
|---|---|---|
| KCl-LiCl | 2.74 | 2.26 |
| KCl-NaCl | 2.74 | 3.11 |
| KCl-$ZnCl_2$ | 2.74 | 7.26 |

Even though enhanced activity could be obtained (14%) on the CN-KCl-NaCl due to the improved optical property, the activity improvement was not as high as that of the CN-KCl-LiCl since it has low crystallinity and low surface area. As for the CN-KCl-$ZnCl_2$, it gave even lower activity than the CN (7%). Different from other CN samples, the CN-KCl-$ZnCl_2$ showed a decrease in the intensity of C-N groups and the existence of Zn species in the CN network as reflected in its DR UV-vis spectrum. This might imply that the large defect formation on the CN-KCl-$ZnCl_2$, as also supported by its FTIR spectrum, would result in the deterioration of the photocatalytic performance.

The activity of the CN could be considered low as compared to the benchmark titanium dioxide ($TiO_2$) photocatalyst that is highly active for degradation of phenol under UV light irradiation.[29] However, it is worth noting here that the ability of the CN to harvest the visible light is very crucial for the application of using sunlight energy. Hybrid materials between CN and other materials have also been reported.[27,28,30] For instance, the activity of the CN for degradation of phenol under visible light irradiation for 5 h could be improved up to 1.3 times higher with the presence of zinc oxide.[27,28] On the other hand, the use of reduced graphene oxide-carbon nitride could have up to 2.8 times higher photocatalytic activity than the CN when the photocatalytic degradation of phenol was carried out under visible light irradiation for 3 h.[30] Since this work demonstrated that 2.4 times higher photocatalytic activity could be achieved on the crystalline CN, better improvement is expected when it is used with other materials as a composite or hybrid photocatalyst.

### 2.6. Conclusions

In summary, a study on the effect of various salt melts, which were KCl-LiCl, KCl-NaCl, and KCl-$ZnCl_2$, for the preparation of CN has been successfully demonstrated. XRD, DR UV-Vis, FTIR, and $N_2$ adsorption-desorption isotherms were deployed to characterize the as-synthesized photocatalysts. XRD patterns demonstrated that only CN prepared in KCl-LiCl showed the crystalline phase and improved structural order, while others remained in amorphous form, suggesting that the KCl-LiCl salt melt played an important role as the reactive solvent in improving the crystallinity of CN. DR UV-Vis analysis showed that the addition of salt melt also improved the visible light absorption of photocatalysts, while FTIR studies demonstrated the successful formation of CN. The $N_2$ adsorption-desorption isotherm studies showed that only CN-KCl-LiCl maintained the high surface area of CN owing to the formation of the porous structure, while CN-KCl-NaCl and CN-KCl-$ZnCl_2$ showed reduced surface areas. Photocatalytic degradation of phenol after 6 h under solar simulator irradiation were

10%, 24%, 14%, and 7% for reference CN, CN-KCl-LiCl, CN-KCl-NaCl, and CN-KCl-$ZnCl_2$, respectively. It turned out that the CN-KCl-LiCl acted as a highly active photocatalyst, the performance of which was ca. 2.4 times better than the reference CN. This study highlighted that the photocatalytic degradation of phenol could be successfully enhanced on the crystalline CN and this could be potentially applied for photocatalytic oxidation of organic pollutants in wastewater treatment.

## 3. Experimental

### 3.1. Chemicals and materials

Potassium chloride (KCl, 95%) and sodium chloride (NaCl, 100.0%) were purchased from Fisher Chemical, while lithium chloride (LiCl, 99.0%) was purchased from Sigma-Aldrich. Zinc chloride ($ZnCl_2$, >97.5%) was purchased from ACROS Organics. Urea ($CO(NH_2)_2$, 99.5%) was purchased from QRëC, while phenol ($C_6H_5OH$, 99.5%) was purchased from Scharlau Chemie (99.5%). Ethanol solvent ($C_2H_5OH$, 99.98%) was purchased from HmBG Chemicals. All the chemicals used in the synthesis procedure were used without any purification.

### 3.2. Synthesis procedure

Urea (30 g) was calcined at 623 K for 6 h to prepare ca. 10 g of a precursor. Two grams of the precursor was dispersed in 30 mL of ethanol and the solution was stirred and heated at 373 K for 1–2 h. The precursor was then ground together with salt melts, for which compositions of the KCl and another salt (M-Cl, M = Li, Na, or Zn) are listed in Table 3. A certain amount of precursor (ca. 7–12 g) was transferred into a crucible and covered with a lid. The crucible was then placed in a furnace and calcined at 823 K. The calcination process was carried out for 4 h and the rate of the heating process was fixed at 2.2 K/min. The final product was removed from the crucible and washed with boiling water before it was isolated via a filtration process followed by drying in an oven overnight at 333 K. The prepared CN samples were labeled based on the salt melt used in the synthesis as CN-KCl-LiCl, CN-KCl-NaCl, or CN-KCl-$ZnCl_2$. The reference CN prepared in the absence of the salt melt was prepared via direct polymerization of urea by heating 30 g of urea under the same heating conditions as mentioned above.[5,22]

### 3.3. Characterizations

The determination of structural properties and crystallinity of all the synthesized CN samples was carried out by XRD using a Bruker AXS Diffrac Plus release 2000 with Cu K$\alpha$ radiation ($\lambda = 0.15148$ nm) and step size of 0.05° in the $2\theta$ range of 10° to 60°. A Nicolet-iS50 FTIR spectrometer was used to investigate the functional groups in the samples. The sample was mixed with potassium bromide (KBr) before it was pressurized to prepare a pellet to be measured by FTIR. DR UV-vis spectra were studied on a Shimadzu UV-2600 spectrophotometer employing barium sulfate ($BaSO_4$) as the reference. The $N_2$ adsorption-desorption isotherm measurements were performed using a Quantachrome NOVAtouch LX4 at 77 K. Prior to measurement, each of the samples was heated to 423 K and put in vacuum conditions for 3 h. The specific surface area was calculated using the BET model, using adsorption data taken in the range of $0.01 < P/P_0 < 0.3$, by Quantachrome TouchWin 1.0 software.

### 3.4. Photocatalytic degradation of phenol

In order to evaluate the photocatalytic performance of all the synthesized CN samples, 0.05 g of photocatalyst was added into 50 mL of aqueous phenol (50 ppm) in a 100-mL beaker. Prior to the photocatalytic reaction,

the solution was stirred in a dark environment for 30 min to reach equilibrium. The reaction was carried out for 6 h under irradiation of a solar simulator (Peccell Technologies, 150-W Xenon short arc lamp, AM 1.5G). The remaining concentration of phenol in the solution was determined by using high-performance liquid chromatography on a Shimadzu Prominence LC-20A equipped with a UV detector. The photocatalytic degradation of phenol (%) was calculated according to Eq. (1):

$$\text{Percentage of degradation } (\%) = \frac{C_o - C}{C_o} \times 100, (1),$$

where $C_o$ refers to the initial concentration of phenol and $C$ refers to the concentration of phenol after 6 h of reaction under solar simulator irradiation.

**Acknowledgments**

Support from the Directorate General of Strengthening Research and Development, Ministry of Research, Technology, and Higher Education of the Republic of Indonesia, via International Research Collaboration and Scientific Publication (PKLN 2018, No. 061/SP2H/LT/K7/KM/2018 and No. 007/MACHUNG/LPPM/SP2H-LIT/II/2018), is gratefully acknowledged. This work was also supported by the Ministry of Higher Education Malaysia and Universiti Teknologi Malaysia via Research University Grant Tier-1 (Cost Center Code: Q.J130000.2526.13H52). The first author would like to acknowledge the financial support from the MyBrain15-MyPhD Scholarship.

## References

1. Cohen, M. L. *Phys. Rev. B* **1985**, *32*, 7988-7991.
2. Naffakh, M.; López, V.; Zamora, F.; Gómez, M. A. *Soft Mater.* **2010**, *8*, 407-425.
3. Cui, Y.; Zhang, J.; Zhang, G.; Huang, J.; Liu, P., Antonietti, M.; Wang, X. *J. Mater. Chem.* **2011**, *21*, 13032-13039.
4. Liu, J.; Zhang, T.; Wang, Z.; Dawson, G.; Chen, W. *J. Mater. Chem.* **2011**, *21*, 14398-14401.
5. Lee, S. C.; Lintang, H. O.; Yuliati, L. *Chem. Asian J.* **2012**, *7*, 2139-2144.
6. Erdogan, D. A.; Sevim, M.; Kisa, E.; Emiroglu, D. B.; Karatok, M.; Vovk, E. I.; Ozensoy, E. *Top. Catal.* **2016**, *59*, 1305-1318.
7. Hassani, A.; Eghbali, P.; Ekicibil, A.; Metin, Ö. *J. Magn. Magn. Mater.* **2018**, *456*, 400-412.
8. Goettmann, F.; Fischer, A.; Antonietti, M.; Thomas, A. *Angew. Chem. Int. Ed.* **2006**, *45*, 4467-4471.
9. Shalom, M.; Inal, S.; Fettkenhauer, C.; Neher, D.; Antonietti, M. *J. Am. Chem. Soc.* **2013**, *13*, 7118-7121.
10. Bhunia, M. K.; Yamauchi, K.; Takanabe, K. *Angew. Chem. Int. Ed.* **2014**, *53*, 11001-11005.
11. Wirnhier, E.; Döblinger, M.; Gunzelmann, D.; Senker, J.; Lotsch, B. V.; Schnick, W. *Chem. Eur. J.* **2011**, *17*, 3213-3221.
12. Chong, S. Y.; Jones, J. T.; Khimyak, Y. Z., Cooper, A. I.; Thomas, A.; Antonietti, M.; Bojdys, M. J. *J. Mater. Chem. A* **2013**, *1*, 1102-1107.
13. Sundermeyer, W. Angew. *Chem. Int. Ed.* **1965**, *4*, 222-238.
14. Sundermeyer, W. *Angew. Chem. Int. Ed.* **1967**, *6*, 90-91.
15. Verbee, W.; Sundermeyer, W. *Angew. Chem.* **1967**, *79*, 860-861.
16. Bojdys, M. J.; Müller, J. O.; Antonietti, M.; Thomas, A. *Chem. Eur. J.* **2008**, *14*, 8177-8182.

17. Busca, G.; Berardinelli, S.; Resini, C., Arrighi, L. *J. Hazard. Mater.* **2008**, *160*, 265-288.
18. Khataee, A.; Eghbali, P.; Irani-Nezhad, M. H.; Hassani, A. *Ultrason. Sonochem.* **2018**, *48*, 329-339.
19. Hassani, A.; Çelikdağ, G.; Eghbali, P.; Sevim, M.; Karaca, S.; Metin, Ö. *Ultrason. Sonochem.* **2018**, *40*, 841-852.
20. Hassani, A.; Khataee, A.; Fathinia, M.; Karaca, S. *Process. Saf. Environ.* **2018**, *116*, 365-376.
21. Chun, H.; Yizhong, W.; Hongxiao, T. *Chemosphere.* **2000**, *41*, 1205-1209.
22. Alim, N. S.; Lintang, H. O.; Yuliati, L. *J. Teknol.* **2015**, *76*, 1-6.
23. Sam, M. S.; Lintang, H. O.; Sanagi, M. M.; Lee, S. L.; Yuliati, L. *Spectrochim. Acta. A Mol. Biomol. Spectrosc.* **2014**, *124*, 357-364.
24. Ham, Y.; Maeda, K.; Cha, D.; Takanabe, K.; Domen, K. *Chem. Asian J.* **2013**, *8*, 218-224.
25. Boyarchuk, T. P.; Khailova, E. G.; Cherginets, V. L. *Electrochim. Acta* **1993**, *38*, 1481-1485.
26. Fettkenhauer, C.; Weber, J.; Antonietti, M.; Dontsova, D. *RSC Adv.* **2014**, *4*, 40803-40811.
27. Hussin, F.; Lintang, H. O.; Yuliati, L. *Mal. J. Anal. Sci.* **2016**, *20*, 102-110.
28. Hussin, F.; Lintang, H. O.; Lee, S. L.; Yuliati, L. *Mal. J. Fund. Appl. Sci.* **2018**, 159-163.
29. Ahmed, S.; Rasul, M. G.; Martens, W. N.; Brown, R.; Hashib, M. A. *Desalination* **2010**, *261*, 3-18.
30. Tiong, P.; Lintang, H. O.; Endud, S.; Yuliati, L. *RSC Adv.* **2015**, *5*, 94029-94039.